Astron. Astrophys. 355, 848–862 (2000)

ASTRONOMY AND ASTROPHYSICS

Abell 521: dynamical analysis of a young cluster⋆

S. Maurogordato[1], D. Proust[2], T.C. Beers[3], M. Arnaud[4], R. Pelló[5], A. Cappi[6], E. Slezak[1], and J.R. Kriessler[7]

[1] CERGA, CNRS, Observatoire de la Côte d'Azur, B4229, Le Mont-Gros, 06304 Nice Cedex 4, France (maurogor@obs-nice.fr)
[2] DAEC, CNRS, Observatoire de Paris-Meudon, 5 place J. Janssen, 92195 Meudon, France (proust@obspm.fr)
[3] Department of Physics and Astronomy, Michigan State University, E. Lansing, MI 48824, USA (beers@pa.msu.edu)
[4] CEA/DSM/DAPNIA/Service d'Astrophysique, CEA/Saclay, 91191 Gif sur Yvette Cedex, France (arnaud@hep.saclay.cea.fr)
[5] Observatoire Midi-Pyrénées, Avenue E.Belin, Toulouse, France (roser@astro.obs-mip.fr)
[6] Osservatorio Astronomico di Bologna, via Ranzani 1, 40127 Bologna, Italy (cappi@astbo3.bo.astro.it)
[7] Department of Astronomy, University of Minnesota, 116 Church St. S.E., Minneapolis, MN 55455, USA (jeffk@isis.spa.umn.edu)

Received 22 January 1999 / Accepted 4 November 1999

Abstract. We present the results of a dynamical analysis of the rich X-Ray luminous galaxy cluster Abell 521, and discuss the nature of the arc-like structure first noted by Maurogordato et al. (1996). Our study is based on radial velocities for 41 cluster members, measured from spectra obtained at the European Southern Observatory and the Canada-France-Hawaii Telescope. Based on statistical analyses performed with the ROSTAT package, we find that Abell 521 is an intermediate-redshift cluster ($C_{BI} = 74132^{+202}_{-250}$ km s^{-1}) with a rather high apparent value of the velocity dispersion $S_{BI} = 1386^{+206}_{-139}$ km s^{-1}.

There are many indications that this cluster is presently undergoing strong dynamical evolution: a) the high value of the velocity dispersion, which cannot be explained by trivial projection effects, b) significant clumping in the two-dimensional projected positions of the galaxies in the cluster, as quantified by a mixture-model three-group partition significant at the 99 % level, c) the extreme value of the velocity dispersion ($\sigma \sim 2000$ km s^{-1}) in a central high density NE/SW structure, d) a strong increase of the velocity dispersion as determined from the reddest and bluest galaxies, suggesting that cluster spirals are not yet virialized, e) the presence of multiple nuclei in the core of the brightest cluster galaxy as well as clear signatures of interaction effects, and f) an apparently different stellar population for the various knots of the arc candidate which changes along the structure.

The two brightest knots of the giant arc candidate are shown to be at the velocity of the cluster. The bright curved structure is thus probably due to interaction processes between the knots rather than due to strong gravitational lensing. However, gravitational lensing might be present in this cluster, as suggested by the colors of two fainter arclet-like structures.

Key words: galaxies: clusters: general – galaxies: clusters: individual: A 521 – galaxies: distances and redshifts – galaxies: kinematics and dynamics – cosmology: observations

1. Introduction

Clusters of galaxies are complex, evolving systems which present numerous observational and theoretical challenges, yet the scientific payoff of a detailed understanding of these structures is also great. The determination of the total gravitationally-bound mass, the relative distribution of visible (galaxies and hot gas) and dark matter, and the dynamics of galaxies in clusters all provide essential information for testing models of galaxy formation and evolution.

There exist numerous uncertainties in deriving estimates of the mass distribution within clusters from optical observations alone (Merritt & Gebhardt 1995). X–ray observations of the hot gas in clusters permit significant progress in our understanding of cluster dark matter distributions. The two approaches are complementary, but for both methods strong assumptions are required for recovering the mass distribution. The optical approach (through the virial analysis) requires one to adopt hypotheses concerning the orbital distribution of member galaxies, while the X–ray approach assumes that the hot gas is in hydrostatic equilibrium within (presumably) a single cluster gravitational potential. A comparison of both methods, when possible, provides the opportunity to test the underlying hypotheses and to better constrain the model parameters (Henry et al. 1993). With this aim in mind, we have initiated a combined X–ray and optical observational program, including both imaging and multi–object spectroscopy at ESO and at the CFHT, for a selected sample of clusters at intermediate redshifts. Our sample was defined in order to cover a variety of clusters, which could be taken as representative of a range of dynamical states.

Abell 521 is a distant (Abell distance class 6), relatively rich (Abell richness class 1), southern cluster, morphologically classified as Bautz-Morgan Type III (Abell 1958; Abell et al. 1989). This cluster was shown by the HEAO-1 survey to be a

Send offprint requests to: Sophie Maurogordato

⋆ Based on observations made at the Canada France Hawaii Telescope (CFHT) and at the European Southern Observatory. CFHT is operated by the National Research Council of Canada, the Centre National de la Recherche Scientifique of France, and the University of Hawaii.

bright X–ray source (Kowalski et al. 1984). In images taken to select spectroscopic targets in the field of this cluster, we detected several arc candidates (Maurogordato et al. 1996). This was not surprising, as it is suggested by theoretical studies of the gravitational lensing phenomenon that luminous arcs should be frequently found in the centers of distant X–ray luminous clusters (Le Fèvre et al. 1995). The detection of luminous arcs in Abell 521, *if real*, is important because they provide an independent means to estimate the *total* mass of the cluster, without requiring explicit models of the mass distribution (Fort & Mellier 1994). We were thus motivated to focus on this cluster for further analysis, mainly through multi-object spectroscopy, to probe its dynamical state, with long-slit spectroscopy, to test the reality of the arc and arclet candidates, and with multi-band photometry of the central region, with X–Ray imaging and spectroscopy being conducted in parallel. The combined X–ray and optical analysis of the cluster will be presented in Arnaud et al. (2000); a photometric redshift analysis of the arc candidates from multicolor photometry will appear in Pelló et al. (2000).

Sect. 2 of this paper presents the spectroscopic data we have obtained to date in our observational campaign. Sect. 3 is an analysis of the velocity distribution. In Sect. 4 we discuss the nature of the brightest cluster galaxy, and the reality of the gravitational arc candidates which have been previously suggested. In the following, unless explicitly specified, we have used $H_0 = 50\mathrm{h}_{50}\,\mathrm{kms}^{-1}\mathrm{Mpc}^{-1}$, and $q_0 = 0.5$.

2. Observations and data reduction

Multi-object spectroscopic observations of Abell 521 were carried out at the ESO 3.6m telescope in December 1995 and at the CHFT in March 1997. At ESO, we used the Faint Object Spectrograph and Camera with the grism O300, yielding a dispersion of 230 Å/mm, and the TEK512 CCD chip (27 μm 512 x 512 pixels); at CFHT we used the Multi Object Spectrograph facilities (Le Fèvre et al. 1994) with the grating O300, resulting in a dispersion of 240 Å/mm, and the STIS2 CCD (21 μm 2048 x 2048 pixels). These combinations of gratings and detectors result in dispersions of 6.3 Å/pixel and 5 Å/pixel, respectively. Typically, two exposures, of 2700 s each, were taken for fields across the cluster. Wavelength calibration was done using arc lamps before each exposure (Helium–Argon, and Helium–Neon lamps). Data reduction was carried out with IRAF[1], using the MULTIRED package (Le Fèvre et al. 1995). Radial velocities were determined using the cross–correlation technique (Tonry & Davis 1981) implemented in the RVSAO package (developed at the Smithsonian Astrophysical Observatory), with radial velocities standards obtained from observations of late-type stars and previously well-studied galaxies.

We have obtained 65 spectra of objects in the region of Abell 521. Star contamination was very low (only 3 of the 65 targets turned out to be stars). From these data we have retained 49 spectra of galaxies with signal-to-noise ratios sufficiently high to derive a measurement of the radial velocity with good confidence (with the parameter R parameter of Tonry & Davis greater than 3). This results in a completeness of our velocity sample of 30% of the galaxies brighter than $m_V = 21$. The finding chart for the objects with measured velocities is shown in Fig. 1. Spectra of the brightest BCG components were obtained with EFOSC at ESO using the long-slit mode, and 3 different exposures (2×2700 sec and 1800 sec). Imaging of Abell 521 was obtained in 1994 at the CFHT with the MOS in B and R (using the LORAL3 CCD) and in 1997 in the V and I bands (using the STIS2 CCD); the definition and analysis of the galaxy catalog from the V-band image are presented in Arnaud et al. 2000, and the complete photometric catalog will be provided in Slezak et al. 2000. Also, a J-band image of the cluster core was obtained in November 1996 at the CFHT with OSIS and 1800 sec of total exposure time (see Pelló et al. 1999). Velocity measurements from our spectroscopy are listed in Table 1. The columns are as follows: column (1): Identification number of each target galaxy in the cluster as shown in the finding chart; Columns (2) and (3): Right ascension and Declination (J2000.0) of the target galaxy; Column (4): Best estimate of the radial velocity resulting from the cross–correlation technique; Column (5): estimated error; Column (6): a listing of detected emission lines. Galaxies numbered 1–21 were observed at CFHT, while those from 22–49 were obtained at ESO.

3. Velocity distribution and dynamics in Abell 521

3.1. Global mean velocity and velocity dispersion of the cluster

From a visual inspection of the cone diagram displayed in Fig. 2, we selected a reasonable range of velocities (70000 to 80000 km s^{-1}) which brackets candidate members of the cluster. One galaxy (number 2) is identified as a clear foreground object. Three background objects are found at a redshift $z \sim 0.295$; others are at redshifts of 0.289, 0.310 0.331 and 0.360.

We have employed the ROSTAT package (Beers et al. 1990, hereafter BFG) to analyze the velocity distribution of the 41 remaining galaxies in the selected velocity range. In order to quantify the central location and scale of the velocity distribution for Abell 521, we have used the resistant and robust biweight estimators (C_{BI} and S_{BI}, respectively) recommended by BFG. For the complete sample of velocities, we obtain $C_{BI} = 74132^{+202}_{-250}$ km s^{-1} and $S_{BI} = 1386^{+206}_{-139}$ km s^{-1}. Estimates of these quantities obtained with alternative estimators show similar values. The one-sigma errors in these quantities are calculated in ROSTAT by bootstrap re-sampling of 1000 subsamples of the velocity data.

In Fig. 3 (top) we show a stripe density plot of the velocity distribution for Abell 521. The velocity histogram, calculated with a binning of 1000 km s^{-1}, is shown in Fig. 3 (bottom), along with a superposed Gaussian of standard deviation 1386 km s^{-1}, shifted to the velocity of the cluster. The radial velocity of the brightest cluster galaxy (hereafter, BCG) is shown with an arrow.

[1] IRAF is distributed by the National Optical Astronomy Observatories, which are operated by the Association of Universities for Research in Astronomy, Inc., under cooperative agreement with the National Science Foundation

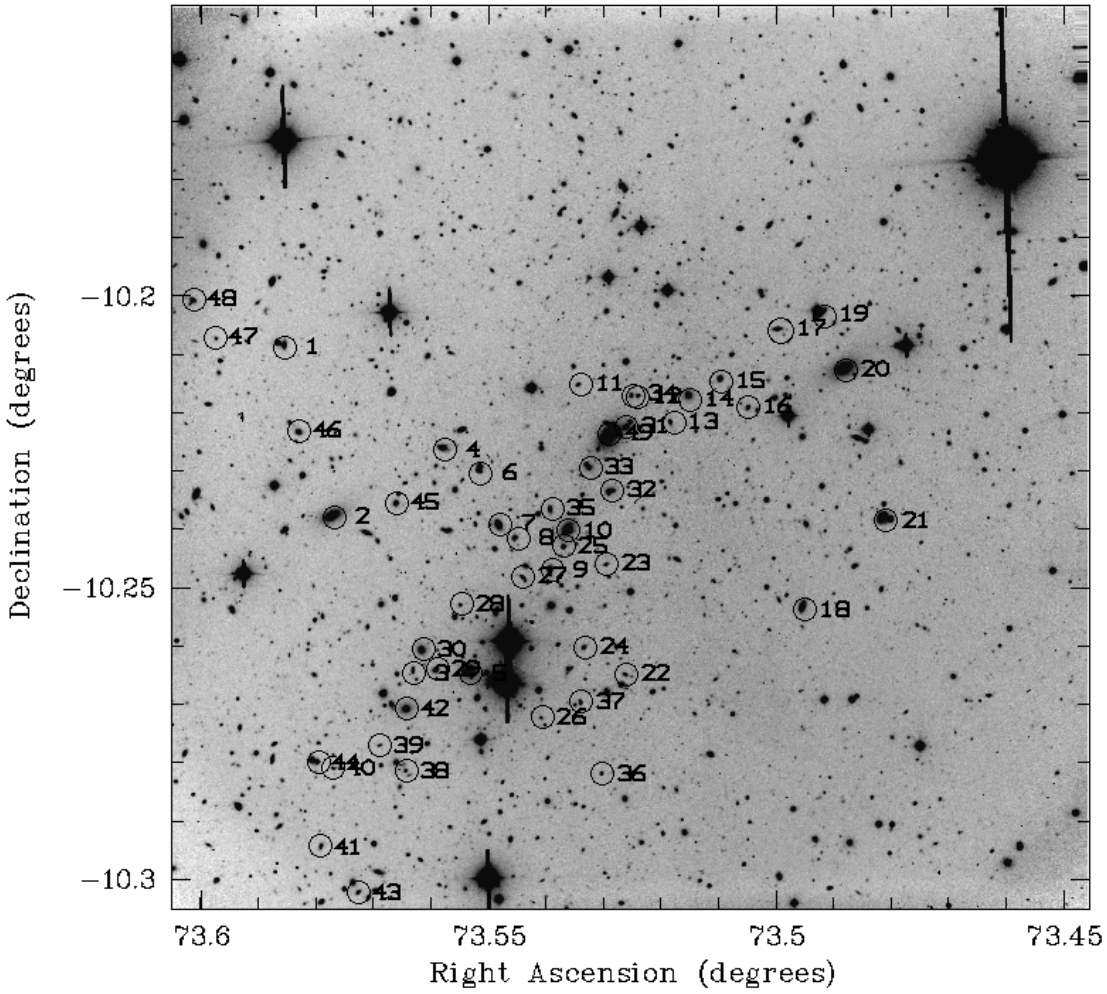

Fig. 1. Finding chart for galaxies with successful velocity measurements in Abell 521. The galaxies are labeled as in Table 1.

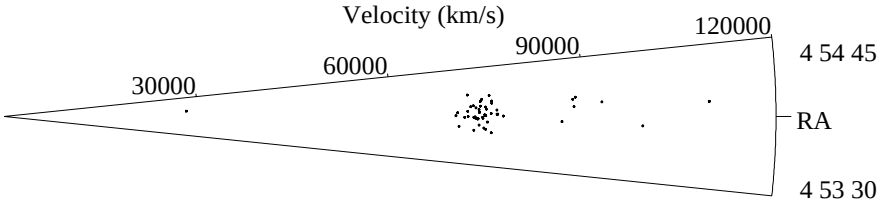

Fig. 2. Distribution in Right Ascension versus radial velocity for 49 galaxies in the inner $10' \times 10'$ region of Abell 521.

The apparent velocity dispersion of Abell 521, $\sigma \sim 1400\,\mathrm{km\,s^{-1}}$, is among the largest values observed in galaxy clusters, as compared, for example, to the velocity dispersion distribution of the recent ENACS survey (Mazure et al. 1996). The dispersion is well above the median value of $744\,\mathrm{km\,s^{-1}}$ estimated by Zabludoff et al. (1990) for a sample of 65 clusters. However, the velocity dispersion of Abell 521 is significantly *larger* than the value ($\sigma = 1017 \pm 65\,\mathrm{km\,s^{-1}}$) we would predict from X–ray observations, using our measurement of the gas temperature, and assuming equipartition between kinetic and potential energy (Arnaud et al. 2000).

We endeavor to determine how reliable this estimate of the velocity dispersion is, and whether or not it is affected by various problems such as subclustering or contamination by outliers. A fair assessment of the impact of potential interlopers is essential for derivation of an unbiased measurement of the velocity dispersion (see for instance Mazure et al. 1996). Given that the spatial coverage of our velocity sample is far from complete, and strongly favors the high-density regions of the cluster, and the limitations imposed by the relatively small number of measured velocities, we cannot proceed to a sophisticated analysis of subclustering. For the present we limit ourselves to classical tests which examine whether our velocity measurements are drawn from a single parent population, or are drawn from a mix of slightly-offset velocity distributions which, taken as a single kinematic entity, would mimic this large velocity dispersion.

Table 1. Heliocentric redshifts in the $10'$x$10'$ frame centered on Abell 521.

NUMBER	**R.A.** (2000)	**DEC.** (2000)	**HEL. VEL.** v (km s^{-1})	**ERROR** Δ v (km s^{-1})	**emission lines**
1	4:54:20.5	-10:12:30.8	74298	84	
2	4:54:18.4	-10:14:15.9	28324	24	
3	4:54:15.1	-10:15:52.5	72534	78	
4	4:54:13.8	-10:13:34.2	88586	102	
5	4:54:12.7	-10:15:52.3	73805	38	
6	4:54:12.3	-10:13:48.4	76607	57	
7	4:54:11.5	-10:14:20.5	72071	54	
8	4:54:10.7	-10:14:28.9	73885	73	
9	4:54:09.3	-10:14:48.4	76630	48	
10	4:54:08.6	-10:14:24.3	74763	53	
11	4:54:08.1	-10:12:53.8	74873	67	
12	4:54:05.7	-10:13:01.4	73640	64	
13	4:54:04.2	-10:13:17.3	86725	206	
14	4:54:03.5	-10:13:02.9	75146	59	
15	4:54:02.2	-10:12:51.8	99306	33	[OII],H_β,[OIII]
1 6	4:54:01.1	-10:13:07.9	73837	89	
17	4:53:59.7	-10:12:19.9	70699	72	
18	4:53:58.7	-10:15:13.0	74604	63	
19	4:53:57.9	-10:12:11.1	74846	93	
20	4:53:57.0	-10:12:44.9	73044	90	
21	4:53:55.3	-10:14:17.9	75759	56	[OII]
22	4:54:06.2	-10:15:53.1	73317	81	
23	4:54:07.0	-10:14:44.8	71584	79	
24	4:54:07.9	-10:15:36.4	77596	38	
25	4:54:08.8	-10:14:33.9	74727	40	
26	4:54:09.7	-10:16:19.8	75692	94	
27	4:54:10.5	-10:14:52.6	70522	112	[OII]
28	4:54:13.1	-10:15:09.7	75002	88	
29	4:54:14.1	-10:15:50.1	73381	57	
30	4:54:14.7	-10:15:37.7	74874	36	
31	4:54:06.2	-10:13:19.8	74435	42	
32	4:54:06.8	-10:13:59.4	73025	51	
33	4:54:07.7	-10:13:44.9	72150	61	
34	4:54:05.9	-10:13:00.2	73704	93	
35	4:54:09.3	-10:14:10.7	76736	76	
36	4:54:07.2	-10:16:54.3	73219	60	
37	4:54:08.1	-10:16:10.0	70225	97	[OII]
38	4:54:15.4	-10:16:52.5	109645	74	
39	4:54:16.5	-10:16:37.0	92925	150	[OII]
40	4:54:18.5	-10:16:51.4	88450	85	[OII]
41	4:54:19.0	-10:17:39.4	75852	52	
42	4:54:15.4	-10:16:14.4	74055	80	
43	4:54:17.4	-10:18:08.0	75799	62	
44	4:54:19.1	-10:16:47.3	74073	74	
45	4:54:15.8	-10:14:07.2	72967	84	
46	4:54:19.9	-10:13:22.7	88820	41	[OII]
47	4:54:23.4	-10:12:24.7	75428	86	
48	4:54:24.3	-10:12:01.1	72048	82	
49	4:54:06.9	-10:13:24.7	74374	47	

3.2. Simple statistical tests of the velocity distribution

We have performed a number of statistical tests of the velocity data for Abell 521. All twelve of the simple tests implemented in ROSTAT are consistent with the hypothesis that the velocities are drawn from a Gaussian parent population. We also searched for the existence of statistically significant gaps in the velocity distribution, which can indicate the possible presence of subclustering, especially when located in the center of a distribution – none were found. Bird & Beers (1993) discuss alternative measures of the classical coefficients of skewness and kurtosis,

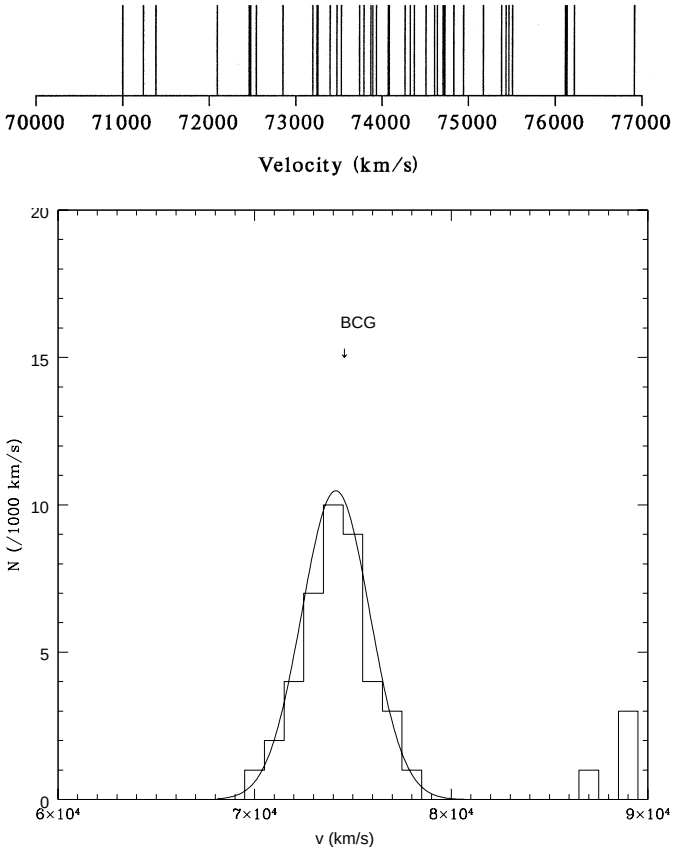

Fig. 3. (Top) Stripe density plot of radial velocities for presumed members of Abell 521. The velocity of the BCG is shown with an arrow. (Bottom) The radial velocity histogram, calculated with a binning of $1000\,\mathrm{km\,s^{-1}}$, in a $10'$ x $10'$ region centered on Abell 521. A Gaussian of standard deviation $1386\,\mathrm{km\,s^{-1}}$, shifted to the velocity of the cluster, is superposed.

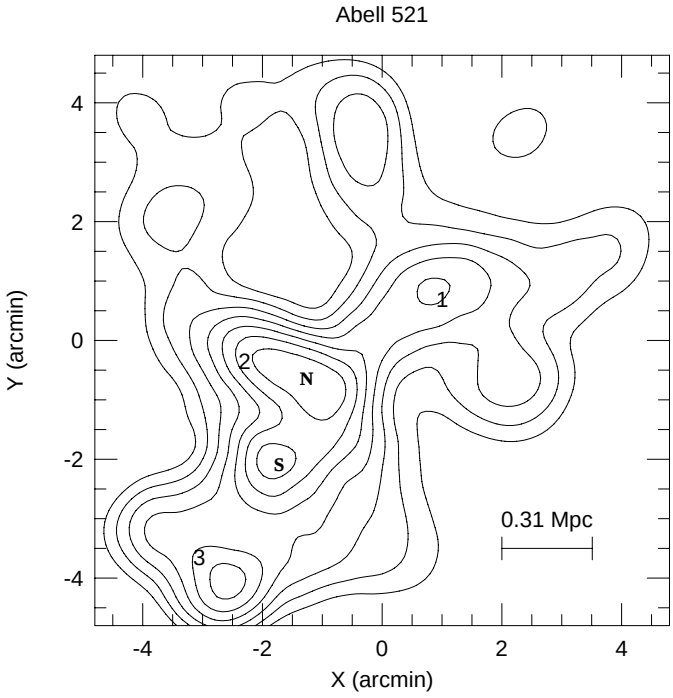

Fig. 4. Adaptative kernel contour map of the projected galaxy distribution for galaxies brighter than $m_V = 22.0$. The centers of the three subclusters corresponding to the KMM best partition are numbered as in Table 2. The minimum contour corresponds to a level of 3.638 galaxies/arcmin^2; the contours are linearly spaced with a separation of 1.073 galaxies/arcmin^2.

the asymmetry index (AI) and the tail index (TI), which are useful for detecting subtle deviations from normality in distributions. For the complete velocity set, we obtain $AI = -0.238$ and $TI = 1.165$, respectively. Neither of these values allow rejection of a Gaussian parent population according to the tables supplied by Bird and Beers (1993).

While we cannot exclude some contamination from outliers or groups along the line-of-sight to Abell 521, these results do exclude the presence of significant projection effects in velocity space.

3.3. Testing for substructure in the projected spatial and redshift distribution

To search for the presence of substructure in the projected spatial distribution of galaxies in Abell 521 we have fit the observed galaxy positions to a number of Gaussian mixture models, following the procedures described in Kriessler & Beers (1997). In this analysis we have only used the ~ 400 galaxies brighter than $m_V = 22.0$, to limit contamination from background galaxies projected on the face of the cluster. Fig. 4 shows an adaptive-kernel contour map of the region centered on Abell 521.

The best-fit KMM partition of the projected galaxy positions, evaluated using a maximum-likelihood ratio test and a bootstrap procedure, is a three-group partition which is significant at the 99% level (parameters of the partition are specified in Table 2). Column (1) of this table lists the identification number of the group (indicated in Fig. 4). Column (2) lists the number of galaxies assigned to each group. Columns (3) and (4) list the fraction of the total number of galaxies present in each group, and the fraction of total luminosity in each group, respectively. The x and y positions of the groups, along with their one-sigma errors, are listed in columns (5) and (6). The median magnitude of the galaxies within each group is listed in column (7); column (8) lists the mean magnitude of the 10th to 20th brightest galaxies in each group. Fig. 5 shows the reconstructed contour maps of the three Gaussians corresponding to the best-fit partition obtained with the KMM algorithm.

From application of a K-S test to the magnitude distributions of the various groups, we find that group 3 is marginally fainter than the others. This, along with the fainter value of m_{10-20} (see Jones & Mazure 1996), suggests that group 3 may contain a large fraction of background galaxies.

We next obtain a split of the velocity sample, assigning each galaxy to a group associated to the nearest projected group center obtained from the KMM analysis. This results in 9 galaxies associated with KMM1, 19 with KMM2, and 2 galaxies with KMM3. Galaxies located farther than 1.5 arcmin from any of the group centers are set aside.

Table 2. Mixture Model Parameters for Abell 521

group	N_g	$\%N_{tot}$	$\%L_{tot}$	$x \pm \sigma_x$ (arcmin)	$y \pm \sigma_y$ (arcmin)	m_{med} (V)	m_{10-20} (V)
(1)	(2)	(3)	(4)	(5)	(6)	(7)	(8)
1	184	46	46	1.8 ± 1.7	0.9 ± 2.4	21.0	19.3
2	160	40	47	-1.6 ± 1.4	0.0 ± 2.3	20.9	19.4
3	52	13	7	-2.4 ± 1.0	-3.4 ± 0.7	21.2	20.7

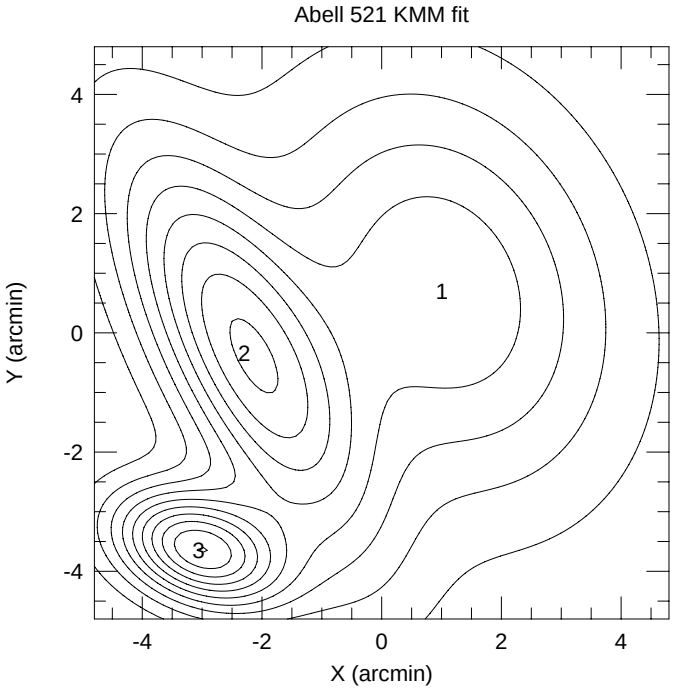

Fig. 5. Reconstructed contour maps of the three best-fit two-dimensional Gaussians obtained from the KMM analysis (Table 2). The minimum contour corresponds to a level of 0.130 galaxies/arcmin^2; the contours are linearly spaced with a separation of 1.329 galaxies/arcmin^2.

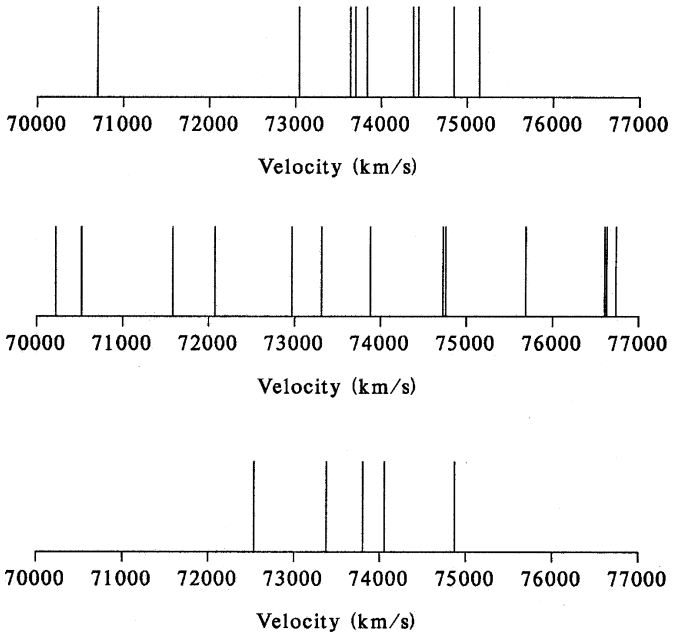

Fig. 6. Stripe density plots of radial velocities for the three partitions analysed with ROSTAT – from top to bottom: KMM1, KMM2 North, and KMM2 South.

Table 3. ROSTAT analysis of velocity samples in Abell 521

sample	N_v	v_{BI}	S_{BI}	AI	TI
All	41	74132^{+202}_{-249}	1386^{+206}_{-139}	-0.24	1.17
KMM1	9	74124^{+289}_{-232}	806^{+682}_{-240}	-0.65	1.74
KMM2 (N)	14	74122^{+552}_{-650}	1994^{+328}_{-226}	-0.37	0.75
KMM2 (S)	5	73751^{+228}_{-390}	747^{+276}_{-57}	-0.11	....
red	19	74125^{+218}_{-273}	1011^{+214}_{-108}	+0.49	1.19
blue	20	73924^{+408}_{-445}	1803^{+256}_{-191}	-0.09	0.96

We then obtain a further split of the KMM2 group into two components: KMM2 North (14 galaxies) and KMM2 South (5 galaxies) in order to isolate the Southern extension of KMM2 seen in the adaptive kernel map shown in Fig. 4. There are only two galaxies with measured velocities assigned to the KMM3 region (numbers 40 and 42), both of which have slightly higher velocities than the adopted central location velocity for the cluster as a whole. More measured velocities are required to reliably determine the mean velocity of KMM3.

We are thus left with three subsamples of the velocity catalog on which we have run the ROSTAT package, corresponding to regions KMM1, KMM2 North, and KMM2 South. The results of this analysis are summarized in Table 3. Although the small number of velocities in each subsample do not allow us to derive precise measurements of the velocity dispersions, two qualitative conclusions can be drawn. First, there are no significant velocity offsets between the individual partitions with respect to one another, at least to within the bootstrapped errors on the velocity locations. Second, the KMM2 North partition has a significantly higher value of the velocity dispersion than the other two partitions, or as compared to the cluster as a whole. This result is also strikingly clear on the stripe density plots of these three partitions displayed in Fig. 6. The KMM2 North group, which includes the so-called "ridge" structure described by Arnaud et al. (1999), is probably kinematically complex, and may well be comprised of several subclusters.

We have also examined the location of the three galaxies with $z \sim 0.295$ (objects 4, 40, and 46) to check if they are spatially clustered, as would be expected for a background group. These galaxies are all located in the Eastern part of the cluster.

Taking into account the velocity measurement in Table 1, galaxies 4 and 46 are separated from one another by $\sim 3.2h_{50}^{-1}$Mpc, and lie at the Eastern part of the KMM2 structure. Galaxy 40 lies $\sim 2.4h_{50}^{-1}$ Mpc from galaxy 4, and $\sim 5.2h_{50}^{-1}$ Mpc from galaxy 46 in the Southern direction. It is thus not excluded that these three galaxies are members of a background loose group, but a much more complete redshift survey of Abell 521 is required to resolve this question.

3.4. Analysis of the velocity distribution with the color index

Several analyses have shown that the velocity distribution of galaxies in clusters can be very different for individual morphological types (e.g., see the analysis by Binggeli et al. 1987 on the Virgo Cluster, Beers et al. 1992 on A400, Bird et al. 1995 on Abell 151, and of Girardi et al. 1996 on a larger sample of clusters). A higher value of velocity dispersion is generally found for late-type galaxies, as compared to early types, which is expected if the latter have fallen into the cluster potential following the initial collapse (Tully & Shaya 1984). The spatial resolution of our imaging data for Abell 521 is unfortunately not sufficient to assign a morphological type to all the objects with measured velocities, in particular at the faintest magnitudes. As an alternative, we have used the color indices of the galaxies in order to define two subsamples within our velocity catalog, with values of $B-R$ respectively higher and lower that the median value for the sample as a whole. In the following we refer to these as the "*red*" and "*blue*" subsamples.

Inspection of the brightest galaxies, whose morphological type is unequivocally determined by eye, shows that typical cluster ellipticals belong to the *red* subsample, and spirals to the *blue* subsample. Galaxies of the cluster with detected emission lines (Table 1) belong to the *blue* subsample, as expected. Fig. 7 shows stripe density plots of the velocity distributions for the *red* and *blue* subsamples. These subsets appear rather different. ROSTAT analysis of the two subsamples yields values of $C_{BI} = 74125^{+218}_{-273}$ km s^{-1} and $S_{BI} = 1011^{+214}_{-108}$ km s^{-1} for the *red* subsample of 19 galaxies, and $C_{BI} = 73924^{+408}_{-445}$ km s^{-1} and $S_{BI} = 1803^{+256}_{-191}$ km s^{-1} for the *blue* subsample of 20 galaxies, respectively. The central locations on velocity of the high and low $B-R$ subsamples are consistent with one another, but the velocity scales are significantly different. We have further checked how stable these results are by testing different subsamples obtained by translating the color cut on $B-R$ within 1σ around the median value. The range is of course limitated, as the number of objects falls rapidly when moving off the median. The values of the dispersions which are obtained fluctuate $\sim 20\%$ around the previously calculated ones, but the general trend is confirmed and becomes even more accentuated when considering the most extreme regions of the color distribution. In any case, the velocity distribution of the *blue* subsample is quite large, while the *red* subsample shows a value which is typical of other galaxy clusters.

One might wonder if the colors of the galaxies are correlated with the high-density structures evidenced in the V-band density map. Based on our inspection of the color indexes, there might be a color segregation in the various structures, with a bluer NE/SW extension including KMM2 North and more compact redder clumps along the NW/SE extension. However the bluest galaxies belonging to our velocity sample are distributed across the entire field of the cluster, so the high velocity dispersion of these galaxies cannot be due solely to the contribution of the KMM2 North region.

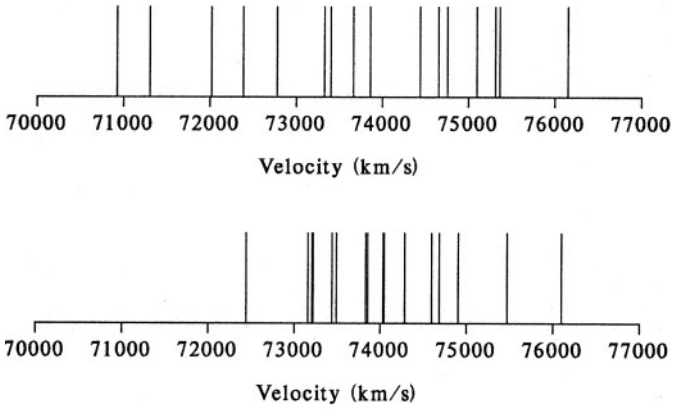

Fig. 7. Stripe density plots of radial velocities for the two subsamples split according color index: (Top) the *blue* subsample, and (Bottom) the *red* subsample.

The higher velocity dispersion of the *blue* subsample can be explained under the hypothesis that Abell 521 is in fact dynamically complex; one might expect this class of galaxies to include many spirals which are not yet virialized within the cluster potential. In this case the distribution of the spirals would be much more dispersed than that of the ellipticals (Girardi et al. 1996). In fact, the velocity dispersion as estimated from the *red* subsample, $S_{BI} = 1011^{+214}_{-108}$ km s^{-1}, is quite in line with the predicted cluster dispersion based on the X–ray analysis, which is at variance with the dispersion based on the entire set of galaxies with measured velocities.

3.5. Virial mass estimate

Based on our existing data, one can naiively attempt to derive a mass estimate for Abell 521. We can, for instance, calculate the virial mass estimator:

$$M_v = \frac{3r_v\sigma_v^2}{G} \tag{1}$$

where σ is the line-of-sight velocity dispersion of the cluster, and r_v the three-dimensional virial radius. The projected mean harmonic separation:

$$R_H^{-1} = \sum_{i<j} \frac{1}{\mathbf{r_i} - \mathbf{r_j}} \tag{2}$$

where the ij sum is done over all pairs, can be used to derive the three-dimensional virial radius from the relation: $r_v = \pi/2R_H$ (Limber and Mathews 1960). However, a number of problems

are present. We have several pieces of evidence that our cluster is currently undergoing strong dynamical evolution and is not yet virialized. It follows that if our measured velocity dispersion is over-estimated by the presence of sub-clustering, the virial estimate of the mass from our measured velocity dispersion will be a large over-estimate of the real value. Another potential problem is that our imaging field is quite small ($1.3h_{50}^{-1}$ Mpc), and the cluster probably extends well beyond the extension of our image. The estimate of R_H may not have reached a stable value, and our measurement of the mass will be an under-estimate of the total value. This problem can be in some cases overrided by considering the ringwise projected harmonic radius (Carlberg et al. 1996), which is less sensitive to the narrowness of the field. Unfortunately, as this method assumes symmetry about the center of the cluster, and has been shown to be biased in the case of a substantially subclustered distribution, we did not feel appropriate to use it for this highly irregular cluster. We have thus limited our analysis to an estimate of the mass within our imaging field. The virial estimate of the mass as applied to a system bounded at a finite radius will be an over-estimate (by at most 50%) of the real mass contained in this radius, due to ignoring the surface term in the scalar virial theorem (Carlberg 1996). We therefore derive a virial estimate of the mass within a radius of $1.3h_{50}^{-1}$ Mpc, which should be an upper bound of the mass within the same region: $M_v[1.3h_{50}^{-1}Mpc] = 3.1 \times 10^{15}h_{50}^{-1}M_\odot$.

4. The BCG complex

4.1. The brightest cluster galaxies in Abell 521

The brightest galaxy in Abell 521 has an asymptotic magnitude $m_V = 17$, which corresponds to an absolute K-corrected magnitude $M_V = -24.69 + 5\log h_{50}$. Two other gE galaxies are present in the core of Abell 521, identified in Fig. 1 as objects 10 and 20, with magnitudes 18.61 ($M_V = -23.04 + 5\log h_{50}$) and 18.57 ($M_V = -23.0 + 5\log h_{50}$), and velocities of 74763 km s^{-1} and 73044 km s^{-1}, respectively. The K-correction for E/SO galaxies is computed using the spectral energy distribution of an old elliptical galaxy and the filter response. The synthetic spectrum was obtained through the GISSEL96 evolutionary code (Bruzual & Charlot 1993), with the Miller & Scalo IMF (1979) and solar metallicity. Our V-band absolute magnitudes have been corrected from extinction using the maps of Burstein & Heiles (1982), giving $A_v = 0.105$, and a standard Milky Way reddening law (Seaton 1979) for the synthetic spectrum.

In their analysis of a statistical sample of 116 nearby Abell clusters, Hoessel et al. (1980) found an average value of $M_V = -22.68 \pm 0.03$ for the cluster BCG's with a dispersion of 0.35 magnitudes within a 16.4 kpc aperture. We have calculated the K-corrected absolute magnitude in this same aperture (4 arcsec at the redshift of Abell 521) and using the same cosmological parameters ($H_0 = 60$ km s^{-1}/Mpc), and we obtained respectively: $M_V = -22.71$, $M_V = -22.42$ and $M_V = -22.51$ for the BCG, galaxy 10, and galaxy 20, which are all within 1.5σ of their findings. Thus Abell 521 includes, besides the BCG, two other giant elliptical galaxies of central absolute magnitude typical of brighter cluster members. These galaxies could be suspected, in the frame of the hierarchical scenario, to belong to the original sub-units which are merging into the present cluster.

4.2. Photometric analysis of the BCG

4.2.1. Morphology of the BCG

In Fig. 8a we show a one arcmin subframe of the 900 s V-band image centered on the BCG in Abell 521. In Fig. 8b, isocontours emphasize the complex morphology of the BCG region. It is a clear case of a BCG with multiple nuclei. The various knots can be classified into two groups. The first class corresponds to relatively faint and small nuclei in the inner region of the BCG (8–25$h_{50}^{-1}kpc$): A2, A3, and A4. The second group, at a larger distance $\sim 35h_{50}^{-1}$ kpc, corresponds to a chain of more extended and brighter knots: B,C,D,E superposed on a diffuse arc-like structure clearly evidenced in Fig. 8a and 8b. This structure spreads over the northwest quadrant more than 10 arcsecs, with a radius of curvature of ~ 7.5 arcsecs, and is nearly centered on the BCG. The largest structure, embedding B,C,D, and E, is detected at 1 σ above the background, and the brightest one, corresponding to the B-C-D region, at 2 σ. Midway between A and D is detected a moderately bright object with very distorted isophotes (Fig. 8b): A1.

Multiple nuclei in brightest cluster galaxies have been shown to be quite a frequent phenomenon. Various systematic studies of samples of BCGs in clusters (Tonry 1985; Hoessel & Schneider 1985) have shown that about 50% of BCGs have at least one extra nucleus within $20h_{50}^{-1}$kpc. Only a small fraction of these occurances have been shown to be attributed to spurious projections. These nuclei are good candidates for being the remnants of galaxies absorbed into the BCG by cannibalism, according to the scenario of Hausman & Ostriker (1978). In order to test whether the nuclei are chance projections or are physically connected to the BCG, information can be derived directly from the redshift measurements (if available), and also from photometry through a search for tidal distorsions (Lauer 1986, 1988) of the isophotes. Nuclei A2,A3, and A4 were too faint and small to be studied in this program; better angular resolution is required. In order to obtain useful spectroscopic information much longer exposure times are necessary.

4.2.2. Surface brightness profile of the BCG

We then computed the surface brightness profile of the BCG. For this purpose we masked every superposed object up to an angular distance of 100 arcsec from the center of the BCG. We then fit ellipses of constant intensity to the galaxy, as described in Slezak et al. (2000). Intensities and surface brightness have been calculated and compared in twelve quadrants centered on the BCG. Only the quadrants which are not contaminated by the various nuclei have been kept for the final profile, plotted in Fig. 9. The surface brightness profile has been very successfully fitted, in the range 22–27 mag arcsec^{-2}, by a de Vaucouleurs

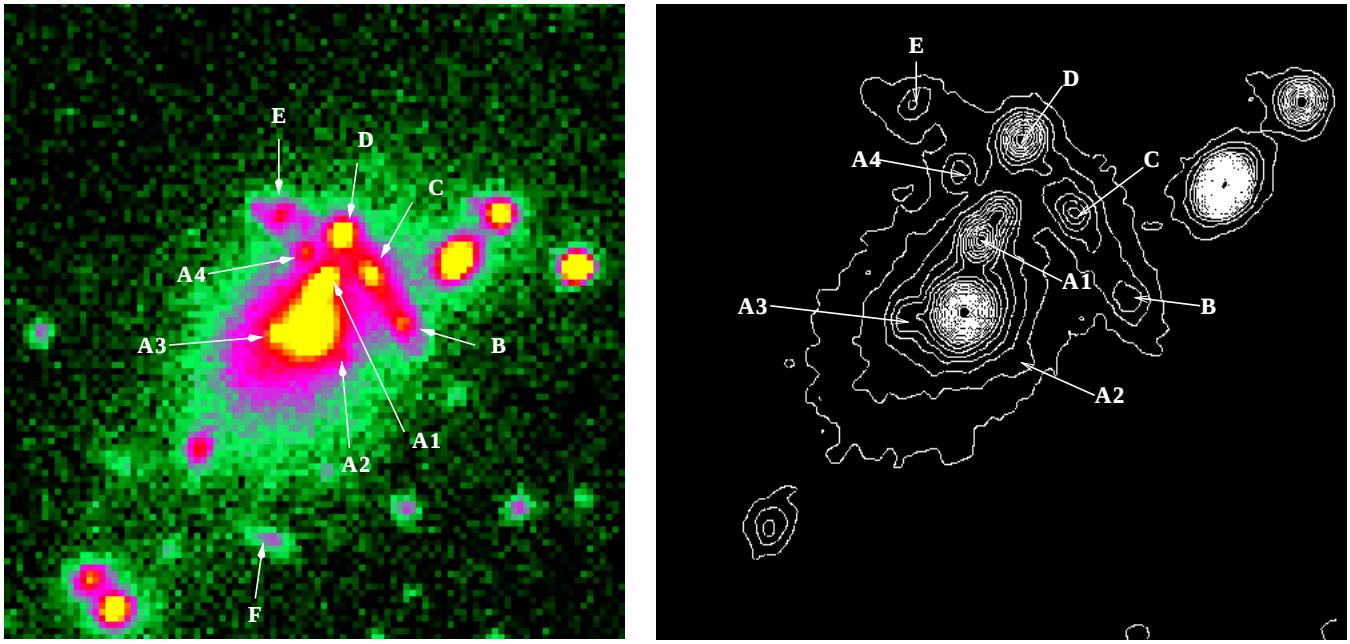

a b

Fig. 8. a: Close-up of a 900 s V-band image of the region of the Brightest Cluster Galaxy in Abell 521 taken at CFHT in March 1997. Multiple nuclei are apparent near the central galaxy A (e.g., A1, A2, A3, and A4). The giant arc candidate is visible to the northwest, at a distance of ~ 7 arcsec from the BCG galaxy, as a diffuse structure with brighter knots superposed (B, C, D, and E). A smaller arc candidate (F) is visible at 14 arcsec to the South. **b**: Isocontours of the BCG complex. The arclike structure is still very apparent. Note the distortion of the inner nucleus A1. The lowest contour corresponds to 1σ above the mean background; contours are spaced by 1σ.

law with $r_e = 10.67$ arcsec (which corresponds to $r_e = 52h_{50}^{-1}$ kpc at the redshift of the object) and $\mu_e = 24.95$.

Although the high value of r_e and the large luminosity which we obtain are quite characteristic of a cD galaxy, we fail to detect the extended luminous envelope which is generally observed as a flattening of the slope in the surface brightness profile at large radius (Matthews et al. 1964; Tonry 1987; Schombert 1988). Since at a surface brightness of $27\mathrm{mag\ arcsec}^{-2}$ our photometry reaches 0.3% of the sky background, it seems quite unlikely that and extended halo could have been missed. This situation is reminiscent of the BCG galaxies in poor clusters analysed by Thuan & Romanishin (1981), which do not show the diffuse halo of cD galaxies in bright clusters. The BCG in Abell 521 seems also to share some other properties with these objects, for instance the large value of effective radius, the relatively low surface brightness, and the quite high total luminosity. If we take for M^* the value estimated by Trevese et al. (1996): $M_F^* = -22.66 \pm 0.45$ (obtained from a photographic sample of 36 clusters obtained with the Palomar 1.2m Schmidt telescope), and convert to V-magnitudes with their color transformation $F = V + 0.76$, we obtain $M_V^* \sim -21.90$. This results in a difference in absolute magnitude $M_V^{BCG} - M_V^* \sim -2.79$ and a total V-luminosity expressed in L_V^* units: $L_V^{BCG} \sim 13 L_V^*$. The two brightest ellipticals (object 10 and 20) have $L_V \sim 2.8 L_V^*$. Galaxy 10 shows a second nucleus in its South-West periphery, but the resolution of our data is not sufficient to rule out a possible projection effect.

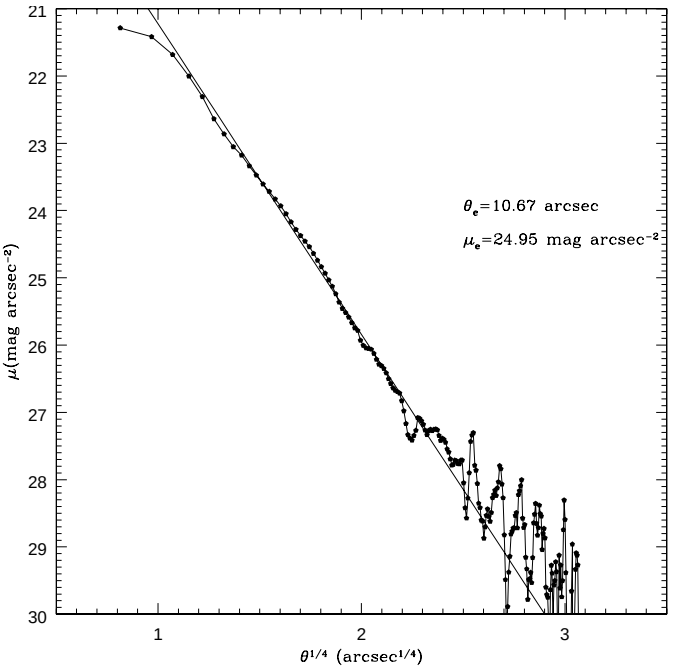

Fig. 9. V-band surface brightness profile of the BCG in Abell 521. The best-fit de Vaucouleurs profile is plotted as a continuous line.

The huge value of L/L^* for the BCG galaxy can be compared to the typical value of ~ 3–4 for rich clusters (without the

envelope) and $\sim$ 6–7 for poor clusters (Thuan & Romainshin 1981). In the case of poor clusters, the merging rate is quite fast due to the compactness of the cluster, but the tidal stripping rate is slower than in the richer ones because of the lower velocity dispersion. It is expected that for these clusters the halo component of of the BCG, which is supposed to form by accretion of tidal debris from galaxy collisions, has not yet had the time to form. If the BCG of Abell 521 were at the bottom of the potential well of the entire cluster, and if the huge *apparent* velocity dispersion derived above were the signature of this cluster being very massive, we would expect it to exhibit a significant extended halo, as in the case of Abell 1413. The fact that multiple nuclei exist and that no halo is detected suggests that the BCG is associated with a smaller component of the cluster with low mass, and hence merging is very efficient but the extended halo has not yet had time to form.

4.2.3. Interaction signatures

We next searched for signatures of interaction between the nuclei of the BCG. In an intensive photometric study of 16 multiple-nucleus brightest cluster galaxies, Lauer (1988) has shown that several typical effects could be detected. These include, for example, tidally induced isophote stretching or twisting, displacements of the isophote centers as a function of the radius, truncation or distension of their envelopes, tidal limiting of secondaries, and the detection of faint features as tidal plumes or dynamical friction wakes.

For this purpose, we have tried to fit elliptical isophotes to the various nuclei of the BCG region. This was done with the ELLIPSE package in STSDAS. Center coordinates, ellipticity and position angle are left as free parameters starting from initial reasonable input values. As a first result, the BCG and knots B,C,D can successively be fitted by ellipses. In the case of the BCG, we have detected a substantial increase of the ellipticity inwards-outwards (Fig. 10a), as well as a twist of the isophotes (Fig. 10b). The isophotes appear concentric within the errors. Unfortunately, with our poor angular resolution, the core of the knots B, C, and D are poorly resolved, and their small extent is only covered by a few pixels. We are therefore not able to derive constraints from the shape of their profiles. Although object D appears circular, objects B and C are elongated in the same direction as the arclike structure (Fig. 8b).

Objects A1 and E could not be fit adequately by ellipses. The isophotes of object A1 are strongly distorted and show a northern tail (Fig. 8b), which suggests that this object is currently interacting with the BCG core region A. (Fig. 10b).

These results suggest that there are at least two main areas where interaction is present in the BCG region– the region surrounding the A1 object and the area embedding the B-C-D complex.

4.3. The giant gravitational arc candidate revisited

We next re-examined the hypothesis that the diffuse curvilinear structure embedding B, C, and D is due to a giant graviational

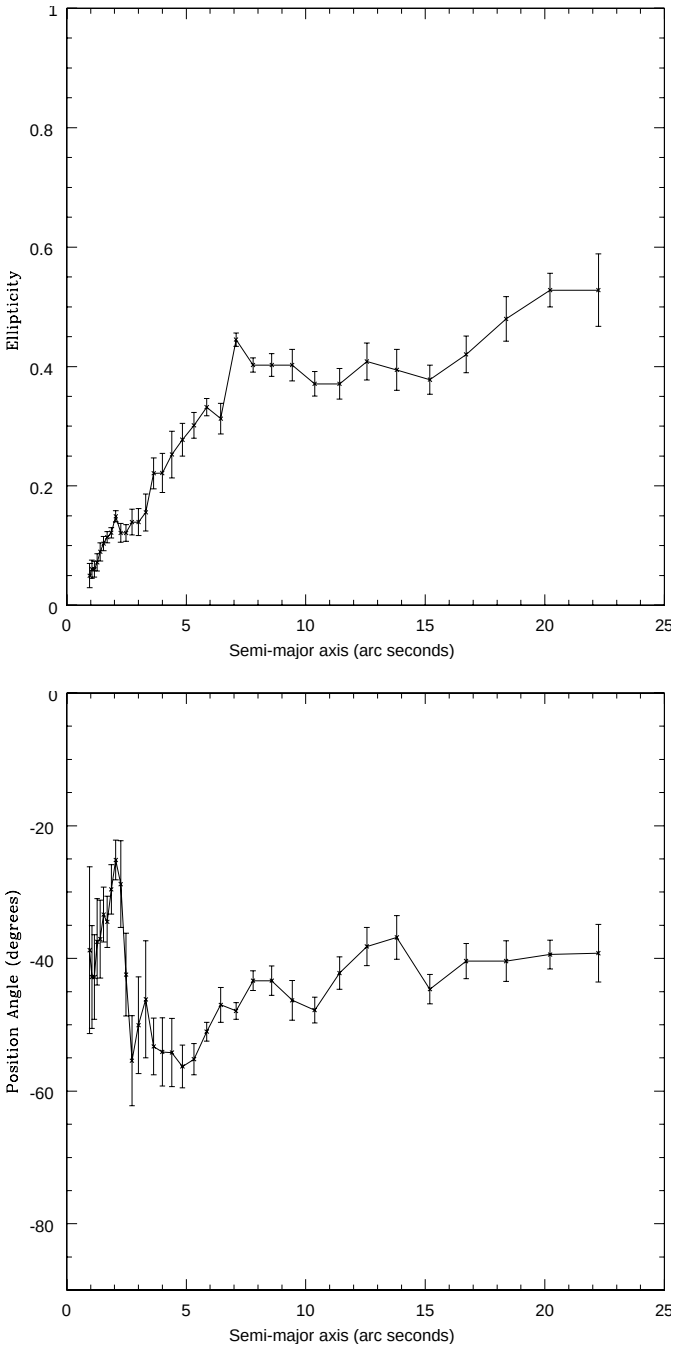

Fig. 10. Variation of the ellipticity (top) and of the position angle (bottom) as a function of the semi-major axis of the fitted ellipse.

arc, as proposed by Maurogordato et al. 1996, by consideration of the spectra and color indices obtained for the various components in the region. The mean magnitudes and colors for the central galaxy and the different knots found in this area are listed in Table 4. The colors of the brightest knot, D, are fully compatible with the expected value for an elliptical galaxy at the cluster velocity, and are also in good agreement with the colors observed for the brightest galaxies in the cluster core. The velocity of this object ($74379 \pm 72\,\mathrm{km\,s^{-1}}$) clearly identifies it as a cluster member. A moderate signal-to-noise spectrum of

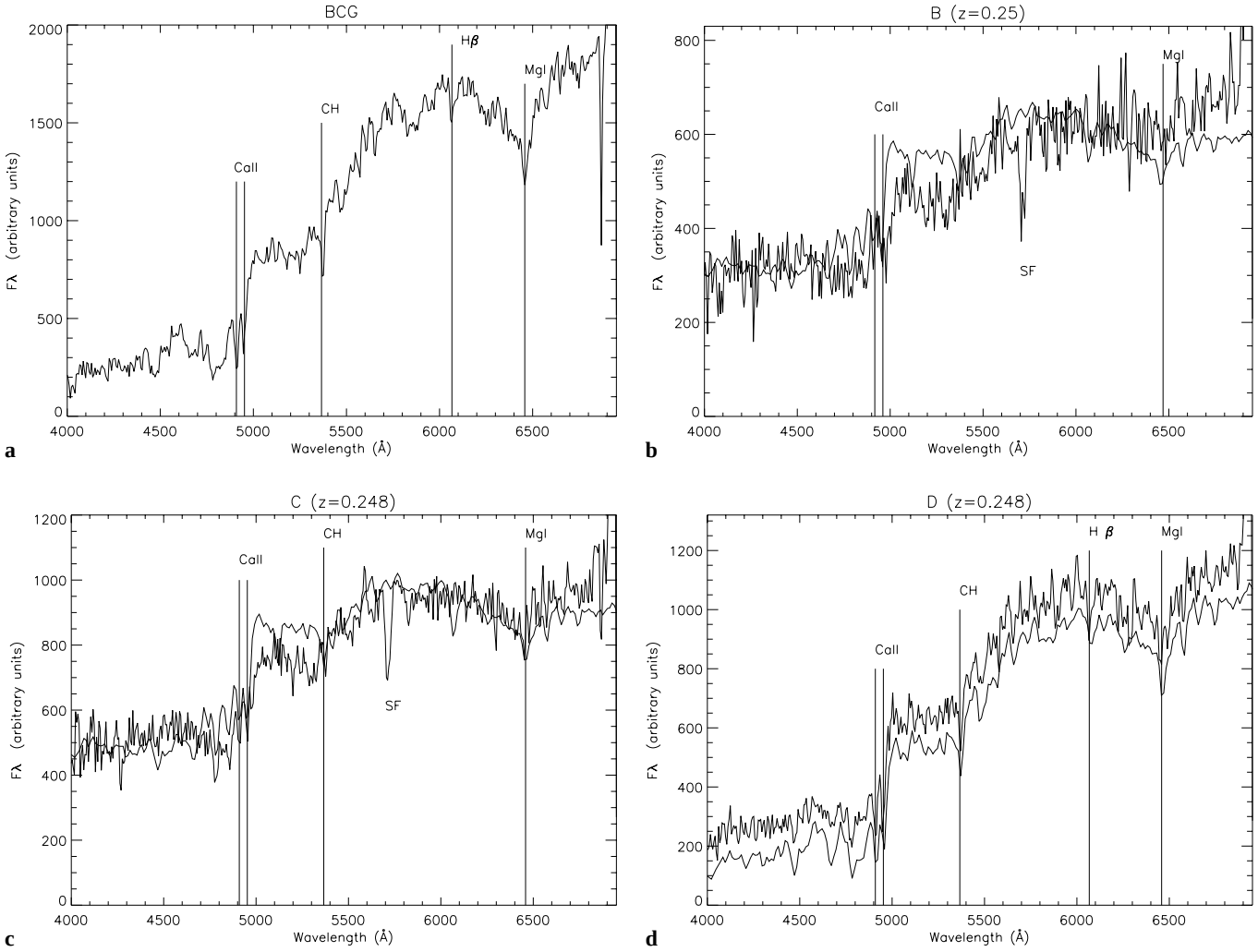

Fig. 11a–d. Spectra of the BCG **a**, and of the various bright components of the arc: knot B **b**, knot C **c**, and Knot D **d**. A synthetic spectrum of an S-type galaxy is superposed on the spectrum of B and C for comparison. An E-type synthetic spectrum is overplotted on the spectrum of the bright knot D.

Table 4. Characteristics of the knots around the BCG in Abell 521

knots	R	B	V	J	$B-R$	$B-V$	$V-J$	v (km s^{-1})	Δ v (km s^{-1})
A	17.42	20.41	18.58	15.54	2.99	1.83	3.04	74374	47
A1	19.27	22.24	20.40	16.88	2.97	1.84	3.52	73857	55
B	20.54	22.65	21.54	18.56	2.11	1.11	2.98	75600	600
C	20.17	22.47	21.11	17.99	2.30	1.36	3.12	74370	300
D	19.79	22.50	20.92	17.88	2.71	1.58	3.04	74370	72
E	21.12	22.85	21.91	18.95	1.73	0.94	2.96		
F	22.35	23.69	23.00	21.17	1.34	0.69	1.83		

knot D is presented in Fig. 11, and compared to a synthetic spectrum of a E-type galaxy. The condensations along the arc candidate display different colors in the filter bands available. This fact strongly argues against the hypothesis of a single multiply-image system due to gravitational lensing.

We now compare the spectral energy distribution of the three knots in detail. Because no spectrophotometric standard star was observed during our observing run, we have used the good-quality spectrum of knot D to flux calibrate the other two components (Fig. 11). As knot D exhibits all the spectral features expected for a typical elliptical galaxy, a synthetic E-type continuum was used for this exercise, taken from the GISSEL evolutionary code (Bruzual & Charlot 1993, updated in 1998). Knots C and D have the same redshift within the errors ($z = 0.248$). The spectrum of knot B is noisier, but its redshift is possibly compatible with that of the cluster ($z = 0.25$, see Table 4).

The spectra of these knots become bluer from D to B, as expected from their $B-R$ colors. At the redshift of this cluster, the $B-R$ color index is a good measure of the 4000 Å break for early type galaxies and of the Balmer break for late type star–forming systems. Furthermore, the relative strength of the Balmer absorption lines increases from D to B. Knot C exhibits absorption lines similar to those found in spiral galaxies at such a resolution, whereas knot B displays some stronger Balmer lines. Unfortunately, the poor quality of the knot B spectrum precludes a careful synthesis of the stellar population. Although a more careful analysis of these objects is needed, based on spectra with better signal-to-noise ratios, these preliminary results suggest a variation in the properties of the stellar population along the arc. If one interprets the change in Balmer line strengths as indicative of an age sequence, the mean age of the underlying stellar population increases from B and C to D.

We conclude that the three brightest knots of the arc structure seen in Abell 521 are in fact cluster galaxies. This result does not completely exclude the gravitational lensing hypothesis for the other arclet candidates in this region (E,F). A deep multicolor photometric survey is required for further progress, in particular to identify possible background sources using photometric redshift techniques.

4.4. Alternatives for the arc-like structure

From the previous section, the gravitational lensing hypothesis for the arc seems rather unlikely. We thus consider various alternative hypotheses to explain the arc-like structure and its knots. If, as probable from the redshift measurements of D and C, the whole system is roughly at the same redshift, the diffuse structure can be interpretated as a "bridge" of stellar matter connecting the different knots. Various physical mechanisms can then be invoked to explain it.

For instance, dynamical friction exerted on a satellite galaxy moving in the gravitational field of a giant elliptical galaxy can create overdensities with arclike morphology centered on the giant galaxy. These "dynamical wakes" have been shown both in numerical simulations (Weinberg 1986, 1989) and detected in several BCG of galaxy clusters (Lauer 1986, 1988). In this case, the arc structure in the BCG of Abell 521 might be caused by the system of small galaxies B, C and D orbiting in the potential of the BCG. Another, perhaps more plausible alternative, would be to interpret it as a tidal tail. In fact, interacting galaxies present varieties of tidal morphologies (bridges, tails, shells) similar to the arclike structure in Abell 521 (for instance UGC 7277). These tails are predicted to develop from the matter torn by tidal forces from the previously colliding galaxies, and can include bound structures which might develop into small galaxies (Barnes & Hernquist 1992). The "arcs" created by such tidal debris are expected to be thicker than those caused by gravitational lensing. In our case, if we assume the whole system is at the same velocity as the BCG, its width would be $13h_{50}^{-1}$ kpc and its length $50h_{50}^{-1}$ kpc (from B to D) to 70 h_{50}^{-1} kpc (from B to E). These sizes can be compared to structures in well-known interacting systems such as Arp 299 ($180h_{50}^{-1}$ kpc, Hibbard & Yun 1999). The various knots could be interpretated as remnants of the collision and the arc-like structure as the tidal tail. Knots B and C are likely, as shown by their spectra, to be rather late type objects, and the diffuse structure could result from the collision of their disks. The fact that their orientation is along the arc-like structure also favours this hypothesis. Another possibility would be that the young knots B and C might be small galaxies in formation within the tail. This "propagating" star formation reminds one of the model of Gerola et al. (1983). Several issues are still unclear, however. For instance, in the case of tidal tails, one would expect a counter-structure on the opposite side of the remnant, which is not observed in our images. A small curved extension is detected as object E, but our resolution is too poor to discriminate between a spiral galaxy seen edge-on and a tidal structure. A second fact is that the arc-like structure has a very regular morphology as compared to traditional tidal patterns. This might be explained if one takes into account that the tidal tail is clearly affected by the gravitational field of the BCG, and dynamical friction is expected to circularize orbits.

Table 5. Main quantities of the BCG

μ_e	r_e	$L_V/L_\odot$	σ	$M/M_\odot$	M/L_V
$\mathrm{mag_V} \times \mathrm{arcsec}^{-2}$	h_{50}^{-1} kpc	h_{50}^{-2}	km s^{-1}	h_{50}^{-1}	h_{50}
24.95	52.	6.1710^{11}	368	1.4610^{13}	24

4.5. Dynamical analysis of the BCG complex

We now test, from the velocity data we currently have, which of the nuclei are bound to the BCG. The high S/N ratio of the spectrum of the BCG, combined with the reasonable spectral resolution, allows a measurement of its velocity dispersion: $\sigma = 368 \pm 63 \mathrm{km\,s^{-1}}$ (P.Prugniel private communication). We have used the expression derived by Poveda (1958) to estimate the mass for a system of radial velocity dispersion σ_v whose profile obeys a de Vaucouleurs law:

$$M = \frac{9 r_e \sigma_v^2}{G} \tag{3}$$

As the core of the BCG was not well resolved, we have in this case preferred this technique to the standard core fitting. Table 5 lists the main quantities estimated for the BCG: column (1) and (2): best-fit de Vaucouleurs parameters r_e and μ_e; column (3): total luminosity in the V band; column (4): stellar velocity dispersion column (5): total mass, and column (6): M/L ratio.

We then calculated the kinetic and potential energy inside regions of increasing radius centered on the BCG galaxy. Our spectral resolution was not good enough to measure velocity dispersions for the knots. As near-IR J-band photometry is available for all these knots, we have derived masses from luminosities in J (Table 4), assuming a constant arbitrary $M/L_J \sim 1.6$ according to Moriondo et al. (1998). This filter is less sensitive than the the optical bands to differences in stellar populations, thus allowing a more realiable estimate of the mass through the whole arc. The values found are: $M_{A1} = 4.05 \times 10^{10} M_\odot$, $M_B = 8.60 \times 10^9 M_\odot$, $M_C = 1.45 \times 10^{10} M_\odot$, and $M_D =$

$1.6110^{10} \times M_{\odot}$. The velocity measurement of nucleus A1 ($73857 \pm 55\,\mathrm{km\,s^{-1}}$) shows a significant peculiar motion with respect to the BCG of $-413 \pm 57\,\mathrm{km\,s^{-1}}$ in the local rest frame. High velocities for secondary nuclei in BCGs are not uncommon and could be the result of eccentric orbits (Tonry 1987). However, the strongly distorted isophote of this object suggests that it is currently interacting with the BCG. The previous energy calculation shows it is bound to it. We also find that the various knots B-C-D are bound to the BCG. In the case of B, the conclusion is however hazardous because of the poor quality of the spectrum. The total mass estimated for these components using this approximation is $7.97 \times 10^{10} M_{\odot}$. The mass of the entire group is $1.47 \times 10^{13} M_{\odot}$.

4.6. Peculiar motion of the BCG?

In most theories of BCG formation in clusters, these objects are required to occupy the bottom of the cluster gravitational potential. However, there have been suggestions of evidence for at least some BCGs presenting significant velocity offsets as compared to the velocity location of the cluster as a whole (Oegerle & Hill 1994). It has been pointed out that many of the apparently large peculiar velocities seem to be correlated with the presence of substructure, and have been claimed to represent a signature of recent (or ongoing) subcluster merger events (Bird 1994). At the bottom of the cluster potential the effect of the gravitational redshift becomes non–negligible (Nottale 1983). As shown by Cappi (1995), in rich clusters this effect gives a significant positive velocity difference between the BCG and the cluster and, while in principle detectable only statistically with a large number of clusters, it represents an additional source of uncertainty for the estimate of the BCG peculiar velocity.

Care must be taken when evaluating the significance of a proposed BCG velocity offset (see the discussion in Gebhardt & Beers 1991), taking appropriate estimates of errors in central location on velocity into account. As from the previous analysis (Sect. 4.5), the BCG seems to be associated with a group within Abell 521, we are particularly interested in determining whether a peculiar offset of the BCG velocity with respect to the location of the main cluster does in fact exist. The BCG galaxy of Abell 521 has a velocity $v_{BCG} = 74374 \pm 47\,\mathrm{km\,s^{-1}}$, slightly higher than the central velocity location of the cluster as a whole $C_{BI} = 74132^{+202}_{-250}\,\mathrm{km\,s^{-1}}$. This results in a peculiar velocity $v_{pec} = +242\,\mathrm{km\,s^{-1}}$, which has to be corrected by $(1+z)$ to obtain the peculiar motion in the cluster rest frame: $v_{pec} = +194\,\mathrm{km\,s^{-1}}$. Since we have argued above that the kinematics of Abell 521 may in fact be rather complex, we have also calculated the velocity offset of the BCG with respect to the *red* subset of velocities. After correction to the cluster rest frame, we obtain a similar peculiar velocity: $v_{pec} = +200\,\mathrm{km\,s^{-1}}$.

Are either of the above offsets statistically significant? Gebhardt & Beers (1991) provide a prescription for answering this question, based on a comparison of the measured (rest frame) velocity of the BCG with respect to the biweight estimator of velocity central location for the parent cluster or subcluster, with bootstrapped (90%) confidence intervals on the velocity central location. The 90% confidence interval on velocity location for the entire set of galaxies is $[-398, +327]\,\mathrm{km\,s^{-1}}$; that for the *red* subsample is $[-432, +371]$. The 90% measurement error for the BCG velocity is $\pm 78\,\mathrm{km\,s^{-1}}$. Thus, in both instances, the peculiar velocity of the BCG is completely contained with the 90% interval on central location in velocity space, and neither offset can be considered significant. This probe could be substantially improved by obtaining a larger set of galaxies with measured velocities in Abell 521, in order to shrink the confidence intervals on location in velocity.

We have also calculated the peculiar velocities of the two bright elliptical galaxies (10 and 20) and obtain rest-frame peculiar velocities of $v_{pec} = +506\,\mathrm{km\,s^{-1}}$ and $v_{pec} = -872\,\mathrm{km\,s^{-1}}$, respectively, when compared to the cluster as a whole. When compared to the *red* subsample, the peculiar velocities are $v_{pec} = +512\,\mathrm{km\,s^{-1}}$ and $v_{pec} = -867\,\mathrm{km\,s^{-1}}$, respectively, which are essentially the same. The 90% measurement errors for the observed velocities of these galaxies are ± 88 and $\pm 150\,\mathrm{km\,s^{-1}}$, respectively. The velocity offset of galaxy 10 is thus judged to be statistically significant, when compared to either the entire cluster or the *red* subsample. The 90% confidence interval on the measured velocity fails to overlap with the 90% confidence intervals on the central locations in either instance. An even greater significance is attached to the velocity offset of galaxy 20. The large peculiar velocities of the two bright elliptical galaxies of the cluster could be an indication that they probably originated in different initial subclusters, as has been seen in other clusters (e.g., Abell 2255, Burns et al. 1995). For instance, galaxy 10 could be associated to a sub-component of the KMM2 structure. However, the position of galaxy 20 at the very western end of the KMM1 complex, which is probably associated with the BCG, is more difficult to explain.

5. Discussion and conclusions

From the analysis of our data obtained through multi–object spectroscopy, we have found that Abell 521 is a moderately distant cluster ($z = 0.2467$) with an apparently very large velocity dispersion ($S_{BI} = 1386\ \mathrm{km\,s^{-1}}$). The velocity distribution of cluster members is consistent with sampling from a parent Gaussian population, and the high dispersion does not seem to result from trivial superposition effects. If it was real, this velocity dispersion would be the signature of an extremly massive cluster. However, our analysis suggests otherwise, and indicates that Abell 521 is a highly unrelaxed system. In fact, there do exist several hints that the large apparent velocity dispersion obtained may be due to a superposition of several distinct populations of galaxies. The projected distribution of the galaxy positions in the cluster can be described with a mixture of three two-dimensional Gaussians, a model which is significant at the 99% level. Analysis of the velocity distribution for these partitions shows that the velocity dispersion is very high ($\sim 2000\,\mathrm{km\,s^{-1}}$) in the central North-East/ South-West "ridge" corresponding to KMM2 North, although the dispersion for the smaller samples of galaxies associated with the KMM1 and KMM2 South partitions are more typical of most rich clusters ($\sim 800\,\mathrm{km\,s^{-1}}$). We also find

that the velocity distribution is rather different for subsets of the galaxies selected according to color, with the bluest objects (spirals) showing a high velocity dispersion ($\sim 1800\,\mathrm{km\,s^{-1}}$) and the redder objects (ellipticals) exhibiting a much smaller dispersion ($\sim 1000\,\mathrm{km\,s^{-1}}$). This is another indication that this cluster is dynamically young, with its population of spirals not yet relaxed to the cluster potential. Moreover, the high value of the velocity dispersion as compared to the one expected from the X-Ray Temperature and the σ/T relation suggests that this cluster is far from dynamical equilibrium.

On the basis of our results, we can outline a tentative picture of the dynamical state of Abell 521. In the frame of hierarchical models, the cluster formation process proceeds by merging of smaller units (Frenk et al. 1996). Several pieces of evidence that merging processes are occurring in this cluster have been obtained. First, one can note that the various clumps evidenced on the NW/SE axis (KMM1, KMM2 South, KMM3) are well-defined concentrations. The foreground/background hypothesis is quite improbable, as redshift measurements have shown that all the groups contain several cluster members (although in the case of KMM3 only two redshift measurements exist). We are then probably seeing the early phase of infall of these various groups. According to numerical simulations (Schindler & Bohringer 1993), we should expect that groups are strongly accelerated and their velocity distributions diverge as the merger process proceeds. However, we do not detect any offset of the central velocity locations of the various groups (except possibly KMM3, which could be at a slightly higher velocity of $\sim 75800\,\mathrm{km\,s^{-1}}$ based on the two measured velocities). This implies that either we are seeing the very beginning of the merging and the clumps are still nearly at rest with respect to one another, or we are witnessing a more advanced state but fail to detect the shift of the velocity distributions because the collision axis happens to be mostly in the plane of the sky.

The apparently large velocity dispersion of Abell 521 is due in great part to the contribution of the KMM2 North structure. Its very high velocity dispersion suggests that we are witnessing the collision epoch, at which point numerical simulations show that the dispersion reaches its maximum value, which can be twice the value after the cluster approaches dynamical equilibrium (Schindler & Bohringer 1993). The present data could be explained in a scenario whereby two (or more) subclusters have just collided along an axis which is projected on the sky in the direction of KMM2 North, but with a substantial component along the line of sight. A detailed merging scenario taking into account the whole set of optical and X-Ray properties of this cluster is presented in Arnaud et al. 2000.

The Brightest Cluster Galaxy of Abell 521 is particularly interesting. Its large luminosity and effective radius are characteristic of a cD galaxy, but no extended halo is detected down to our limiting magnitude of 27 mag arcsec^{-2}. The BCG exhibits multiple nuclei, and a particularly puzzling configuration of several knots superposed on a diffuse arc-like structure. Although we failed to measure the redshift of the diffuse structure, the spectra and colors of the knots indicates (at least for two of them) that they belong to the cluster. The diffuse curvilinear structure would then probably result from previous collisions and further interaction between the knots. Several other signs of interactions are present within the BCG– twisting of the isophotes, and the presence of a clearly interacting nucleus (A1). From our dynamical analysis, the BCG and its various nuclei appear to be a bound system. This is probably a young system of small spatial extensions, belonging to KMM1, in which the merging rate is very fast but the halo of the cD has not had yet time to form. The BCG's peculiar velocity of $194\,\mathrm{km\,s^{-1}}$ with respect to the main cluster is judged not to be statistically significant.

From this analysis, Abell 521 seems to be a galaxy cluster currently forming at moderate redshift. If this kind of object is common, it would represent a severe constraint for low Ω value in the hierarchical model of galaxy formation (Richstone et al. 1992; Kauffmann & White 1993). Additional multi-object spectroscopy in order to obtain a complete set of velocity information for galaxies in Abell 521 down to magnitude $m_V = 21$ is planned. This will allow a better determination of the complex dynamical state of this cluster.

Acknowledgements. We would like to thank C. Vanderriest and O.Le Fèvre for the acquisition of the first images of Abell 521 at CFHT. We thank Philippe Prugniel for calculating the stellar velocity dispersion of the BCG with the Hypercat package currently developed at the Observatoire de Lyon. We are very grateful to Marie-Christine Angonin-Willaime, Lia Athanassoula, Alain Mazure, Jean-Marc Petit and Philippe Prugniel for very fruitful discussions on the nature of the arc-like structure and on the dynamics of this cluster. We thank an anonymous referee for his(her) constructive comments and suggestions which allowed us to improve the quality of the paper.

References

Abell G.O., 1958, ApJS 3, 211
Abell G.O., Corwin H.G., Olowin R.P., 1989, ApJS 70, 1
Arnaud M., Maurogordato S., Slezak E., Rho J., 1999, submitted to A&A
Barnes J.E., Hernquist L., 1992, Nature 360, 715
Beers T., Flynn K., Gebhardt K., 1990, AJ 100, 32
Beers T., Flynn K., Gebhardt K., et al., 1992, ApJ 400, 410
Binggeli B., Tammann G.A., Sandage A., 1987, AJ 94, 251
Bird C.M., 1994, AJ 107, 1637
Bird C.M., Beers T., 1993, AJ 107, 1637
Bird C.M., Davis D., Beers T., 1995, AJ 109, 920
Bruzual A.G., Charlot S., 1993, ApJ 405, 538
Burns J., Roettiger K., Pinkney J., et al., 1995, ApJ 446, 583
Burstein D., Heiles C., 1982, AJ 87, 1165
Cappi A., 1995, A&A 301, 6
Carlberg R., Yee H., Ellingson E., et al., 1996, ApJ 462, 32
Fort B., Mellier Y., 1994, A&AR 5, 239
Frenk C., Evrard A., White S., Summers F., 1996, ApJ 472, 460
Gebhardt K., Beers T.C., 1991, ApJ 383, 72
Gerola H., Carnevali P., Salpeter E.E., 1983, ApJ 268, 75
Girardi M., Fadda D., Giuricin G., et al., 1996, ApJ 457, 61
Henry J.P., Briel U.G., Nulsen P.E.J., 1993, A&A 271, 413
Hoessel J.G., Gunn J.E., Thuan T.X., 1980, ApJ 241, 486
Hoessel J.G., Schneider D.P., 1985, AJ 90, 1648
Hausman M.A., Ostriker J.P., 1978, ApJ 224, 320
Hibbard J.E., Yun M.S., 1999, ApJ, in press

Jones B.J.T., Mazure A.. 1996, in Mapping Measuring, and Modell ing the Universe, ASP Conference Series, 94, eds. P. Coles, V. J. Martinez & M.-J. Pons-Borderia (San Francisco: Astronomical Society of the Pacific), p. 197
Kauffmann G., White S.D.M., 1993, MNRAS 261, 921
Kowalski M.P., Ulmer M.P., Cruddace R.G., Wood K.S., 1984, ApJS 56, 403
Kriessler J.R., Beers T.C., 1997, AJ 113, 80
Lauer T., 1986, ApJ 311, 34
Lauer T., 1988, ApJ 325, 49
Le Fèvre O., Crampton C., Felenbok P., Monnet G., 1994, A&A 282, 325
Le Fèvre O., Crampton C., Lilly S.J., Hammer F., Tresse L., 1995, ApJ 455, 60
Limber D.N., Mathews W.G., 1960, ApJ 132, 286
Matthews T.A., Morgan W.W., Schmidt M., 1964, ApJ 140, 35
Mazure A., Katgert P., den Hartog R., et al., 1996, A&A 310, 31
Maurogordato S., Le Fevre O., Proust D., Vanderriest C., Cappi A., 1996, BCFHT 34, 5
Merritt D., Gebhardt K., 1995, XXIXe Moriond Astrophysics Meetings F.Durret, A.Mazure, J.Tran Thanh Van eds, Editions Frontieres, p. 11.
Miller G.E., Scalo J.M., 1979, ApJS 41, 513
Moriondo G., Giovanardi C., Hunt L.K., 1998, A&A 339, 409
Nottale L., 1983, A&A 118, 85
Oegerle W., Hill J., 1994, AJ 107, 857
Pelló R., et al., 2000, in preparation
Poveda, 1958, Bol. Obs. Tonantzintla y Tacubaya, 17:3
Richstone D., Loeb A., Turner E.L., 1992, ApJ 393, 477
Schindler S., Bohringer H., 1993, A&A 269, 83
Schombert, 1988, ApJ 328, 475
Seaton M.J., 1979, MNRAS 187, 73
Slezak E., et al., 2000, in preparation
Thuan T.X., Romanishin W., 1981, ApJ 248, 439
Tonry J., Davis M., 1981, ApJ 84, 1511
Tonry J., 1984, ApJ 279, 13
Tonry J., 1985, AJ 90, 2431
Tonry J.L., 1987, in Structure and dynamics of elliptical galaxies; Proceedings of the IAU Symposium,Princeton, NJ, May 27–31, 1986 (A88-28051 10-90). Dordrecht, D. Reidel Publishing Co., p. 89–96
Trevese D., Cirimele G., Appodia B., 1996, A&A 315, 365
Tully R.B., Shaya E.J., 1984, ApJ 281, 31
Weinberg M.D., 1986, ApJ 300, 93
Weinberg M.D., 1989, MNRAS 239, 549
Zabludoff A., Huchra J., Geller M.J., 1990, ApJS 71, 1